Final Scientific/Technical Report for DOE Grant No. DE-FG02-03ER15466

Awarded to: Purdue University

Project Title: ***CATALYSIS SCIENCE INITIATIVE:*** **Catalyst Design by Discovery Informatics**

PI - W. Nicholas Delgass

Co-PIs: M. Abu-Omar (Chemistry), J. M. Caruthers, F. H. Ribeiro, K. T. Thomson, W. F. Schneider (University of Notre Dame)

Research Associate: G. Medvedev, **Postdocs**: Z. Zhao and Houyu Zhu (Notre Dame)

Students: J. Clay (N. D.), Y. Cui, , T. Gunanskera (Chem.), J. Kim, P. Majumdar, P. Pletcher (Chem.), S. Pradhan, A. Preston (Chem.), S. McDonough (N. D.), P. Mehta (ND), K. Sabnis, K. Steelman (Chem.), J. Switzer, S. Xiong

Collaborators: J. P. Greeley, Purdue University; J. T. Miller, Purdue University; E. A. Stach, Brookhaven National Laboratory; M. Neurock, University of Virginia; Volkan Ortalan, School of Materials Engineering, Purdue University

Contact Information: Forney Hall of Chemical Engineering, Purdue University
480 Stadium Mall Drive
West Lafayette, IN 47907-2100
765 494 4059, FAX 765 494 0805 delgass@ecn.purdue.edu

Budget: $2,100,000

Period of Execution: 9/15/12-9/14/15, **Project Initiation**: 2012 (renewal of grants starting in 2003)

Executive Summary

Catalysts selectively enhance the rates of chemical reactions toward desired products. Such reactions provide great benefit to society in major commercial sectors such as energy production, protecting the environment, and production of food and goods including clothing, tires, and polymer products and thereby contribute heavily to the country's gross national product. While progress in the discovery and application of new catalysts has been steady, the time scale is long, often 10 to 20 years. Our premise is that the level of fundamental understanding of catalytic events at the atomic and molecular scale has reached the point that more predictive methods can be developed to shorten the cycle time to new processes. Our objective in this work has been to develop such methods to accelerate discovery of new or improved heterogeneous and homogeneous catalysts, and we have made important progress toward this goal. The underlying principle of the work has been that the key to understanding and ultimately predicting catalytic systems is discovery of descriptors that are the fundamental drivers of the chemical behavior. Thus, we have focused on how to gather the most useful experimental and theoretical information, how to utilize that information to identify descriptors, and then how to use the descriptors to predict the behavior of yet unmeasured catalysts. From a fundamental point of view, we think that the chemical reaction mechanism, i.e. the sequence of individual reaction steps, and reliable values of the rate and equilibrium constants that control those steps are necessary ingredients of a successful approach. Ability to predict individual rate constants generates the ability to predict not only the overall reaction rate, but also the rates to individual products in a complex reaction mixture and, therefore, the selectivity, i.e. which product will dominate the mixture, often the more important measure of commercial success. The rate and equilibrium constants, in turn, depend on energy barriers to reaction and energies of interaction between reactant molecules and the catalytic sites on which they adsorb. Thus, those energies are the prime targets for quantitative descriptors. In this context, forecasting catalytic properties requires

the use of broadly applicable ability to predict energies and the consequent behavior of a broad range of potential new catalysts.

The field of catalysis can be divided into two regimes: heterogeneous catalysis where the catalyst is a solid and the reaction medium is a liquid or gas, and homogeneous catalysis where the reaction medium is a liquid and the catalyst is dissolved in the liquid, usually as a molecular complex. For the heterogeneous catalysis regime, we have used the water-gas shift (WGS) reaction ($CO + H_2O \rightarrow CO_2 + H_2O$) over supported metals as a test bed. Detailed analysis and strong coupling of theory with experiment have led to the following conclusions:

- The sequence of elementary steps goes through a COOH intermediate
- The CO binding energy is a strong function of coverage of CO adsorbed on the surface in many systems
- In the case of Au catalysts, the CO adsorption is generally too weak on surface with close atomic packing, but the enhanced binding at corner atoms (which are missing bonding partners) of cubo-octahedral nanoparticles increases the energy to a near optimal value and produces very active catalysts.
- Reaction on the metal alone cannot account for the experimental results. The reaction is dual functional with water activation occurring at the metal-support interface.

It is clear from our work that the theory component is essential, not only for prediction of new systems, but also for reconciling data and testing hypotheses regarding potential descriptors. Particularly important is the finding that the interface between nano-sized metal particles and the oxides that are used to support them represent a new state of matter in the sense that the interfacial bonding perturbs the chemical state of both metals atoms and the support atoms in the interfacial region. Some of the first theoretical descriptions of this important chemistry and potential new source of control of catalyst properties are be in preparation for submission.

On the homogeneous catalysis side, we have used single site olefin polymerization as the testbed. This system is important because changes in a single ligand bonded to the catalytically active metal site can alter the rates of individual steps in the polymerization sequence and thereby change the properties of the resulting polymer, potentially improving its value in a hundred million pound per year industry. We have made a major advance in understanding such systems by developing a population balance kinetic model that allows us to predict the molecular weight distribution (MWD) of the product. That, in turn, allows use of MWD data to fit kinetic parameters. By combining monomer loss data, MWD, measurement of the number of working active sites, and polymer end group analysis, we have a rich data set that is highly discriminating of kinetic mechanism. Thus, we have a robust tool for producing high quality, detailed kinetic parameters, which we have used to refine mechanisms presented in the literature and discover relationships between steric and electronic properties of group IV catalysts and individual rate constants in a number of systems. Our recent work on six-coordinate Zr, Ti, and Hf amine bis(phenolate) systems, we have shown that:

- The sterics (bulkiness) of the ligands specifically affect the chain termination reaction
- The electron density on the metal controls misinsertion (flipped orientation) of the olefin into the growing polymer
- Steric effects related to the size of the ortho ligand on the catalyst have been shown to strongly affect its the degree of dormancy, i.e. tendency to stop reacting

- Changes in the size of the amine pendent group on the catalyst can have such a strong effect on chain termination as to change the catalyst from one that produces only oligomers to one that incorporates oligomers in polymer chains to introduce chain branching.

These effects control the length of molecular chains, the number of errors in the regularity of the chains, and the variation of chain lengths in the final product distribution. These characteristics, in turn, determine the properties of the resulting polymer material. Predictive modeling of polymerization process cannot be done without the quantitative rate constant determination that our unique and comprehensive approach has produced. This tool, combined with insights on how catalyst chemistry affects the rate constants, is an important step toward establishing the quantitative relationships between catalyst chemistry and polymer properties that will allow more efficient searches for new catalysts and speed the discovery process.

Thus, in both the heterogeneous and homogeneous catalysis areas, this work has brought important new understanding to the field. The technical effectiveness of our approach is well demonstrated by its success. For heterogeneous catalysis, experimental work alone would have shown the important of the metal-support interface, but the integration of theory with the experiments has allowed deeper understanding of the fundamental source of the effects and shown the path for how to use this understanding for discovery. In the case of homogeneous catalysis, methodology for determination of which reactions are needed to account for the data and the extraction of quantitative values for rate constants for those reactions allows accurate modeling of reaction behavior. This allowed correlation of trends in catalyst properties with alterations of specific rates, thus contributing to a data base that will guide catalyst discovery. While not yet realized, the economic benefits of this approach will come in significantly shortened cycle times for discovery and ability to fill product demand at lower price.

Comparison of Goals and Accomplishments

The overall goal of this research at the outset was the development of a new paradigm for catalyst discovery and optimization through what we call *Discovery Informatics*, a model-based approach to catalyst design. Our plan to reach this objective was to develop experimental and computational tools to create the information rich database from which chemical descriptors and appropriate models could be identified. Our vehicle for application to heterogeneous catalysis was the water-gas shift reaction, and that for homogeneous catalysis was single site olefin polymerization. Specific aims for heterogeneous catalysis were to identify descriptors for the support function and to create a model that links a full set of descriptors to water-gas shift catalytic activity of supported metals, while for homogeneous catalysis they were development of descriptors for the surprising and specific changes in rates constants in the polymerization reaction network for a family of salan-type Zr, Hf and Ti catalysts. Most of these goals have been accomplished. In the heterogeneous catalyst realm we have shown that close and interactive coupling of theory with experiment leads to new understanding and insight. Our approach produced a focus on the metal/support interface for WGS catalysis by supported metals and revealed a richer than expected new chemistry. While we have not yet gained a sufficiently complete model for that chemistry to allow prediction of new materials, we have made important steps in that direction and begun mapping this potential new source of control of catalytic reactions. Full understanding the range and behavior of this interfacial chemistry will have impact on all reactions catalyzed by this class of materials. In the homogeneous realm, we have been able to link catalyst chemistry to specific polymerization reaction steps and to use that understanding to alter the polymer product. This work clearly demonstrates the

power and importance of the kinetic analysis tools and experimental approach that we have developed to verify reaction networks and obtain quantitative rate constants for the individual reaction steps. The approach will have impact on copolymerization as well as a wide range of homopolymers.

Summary of Project Activities

Water-Gas Shift Reaction

While the water gas shift (WGS) reaction has clear impact on energy issues as it is central to the pathway to clean hydrogen, it also serves here as a test bed for discovery of catalyst descriptors and development of *Discovery Informatics*, our model-based approach to catalyst design. Our substantial database of more than 900 experiments shows a number of interesting trends for the WGS reaction, which we have used to generate increasingly comprehensive models. Our focus has been on understanding the role of the support, identifying and quantifying active sites, understanding promotion by added metals, and modeling.

Water Gas Shift Reaction: Pt-Co bimetallic catalysts

The WGS rate per mole of surface Pt (measured with 6.8% CO, 21.9% H_2O, 8.5% CO_2, 37.4% H_2, and balance Argon) for a series of Pt-Co catalysts supported on multi-wall carbon nanotubes (MWCNT) was observed to increase with Co loading to a maximum promotion of 12 times the rate on Co-free Pt/MWCNT and showed a maximum at a Co:Pt atomic ratio of about 3:1, Fig 1.

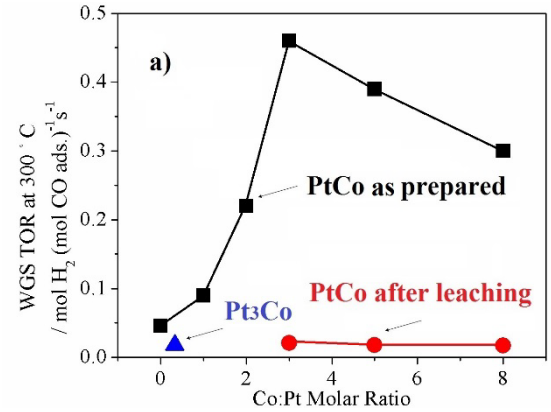

Figure 1. Variation of WGS rate per mole of Pt at 300 ºC with respect to the Co loading.

EXAFS showed that the Pt in all Pt/Co/MWCNT samples was alloyed with Co when the samples were reduced in 25% H_2/Ar at 450°C. The Co-edge EXAFS data showed that in addition to reduced Co, a significant fraction of the Co remained partially oxidized. To selectively remove the excess CoO_x species, we leached them with 5 wt% Acetic acid solution in water. EXAFS confirmed the existence of Pt-Co alloy after leaching. The leached sample showed comparable WGS rates and kinetics with a Co-free Pt/MWCNT sample and with Pt_3Co alloy nanoparticles loaded onto MWCNT. These data confirm the importance of the Pt-CoO_x interface as a promoter to the Pt rate rather than the Pt-Co alloy and a manuscript is being prepared.

Pt_3Re/MWCNT

Similar to Pt_3Co/MWCNT sample, Pt_3Re nanoparticles were also prepared and loaded onto MWCNT. The WGS kinetics are shown in Table 1. The PtRe(1:1) sample was prepared by incipient wetness impregnation. The Pt_3Re sample showed similar promotion compared with PtRe(1:1), suggesting in this case that the alloy may play a role in the promotion.

Table 1. WGS kinetics of PtRe/MWCNT

Sample	Pt Loading /wt%	Test T /°C	WGS Rate per mole of Pt at 300 °C /$10^{-2}s^{-1}$	Ea /kJ(mol)$^{-1}$	H_2O	CO_2	CO	H_2
Pt/MWCNT-r	5	300	1.2	84	0.75	-0.1	0.15	0.30
PtRe(1:1)/MWCNT-r	5	250	4.3	106	0.83	0.06	0.05	0.48
Pt_3Re/MWCNT-r	0.97	280	3.1	100	0.76	0.03	0.10	0.45

Metals Supported on Molybdenum Carbide (Mo_2C)

Two recent papers [Sabnis et al. *J. Catal.* 2015 a and b] show that the 4-5 times higher rates of the WGS reaction over Pt/Mo_2C and PtMo/MWCNT can be attributed to active sites that are formed by Pt-Mo alloy nanoparticles in contact with Mo_2C, not by the formation of the alloy alone. Water activation on Mo_2C is suggested to be the cause for the higher WGS rate over Pt/Mo_2C. Our most recent work on this system has been aimed at low temperature activation. From temperature programmed reaction (TPR) experiments, low surface oxygen content was observed to be crucial for the activity of Mo_2C catalysts. The extent of oxygen removal by 300°C reduction after passivation was significantly higher for Pt/Mo_2C (0.44 ML residual oxygen, 0.98 ML oxygen removed) compared to Mo_2C alone (0.83 ML residual oxygen, 0.69 ML oxygen removed). Thus, even though direct carburization at 600°C produces the best catalyst of this type, promotion of oxygen removal by Pt at 300°C yields a catalyst with specific rate only a factor of 1.8 lower. The finding that the Pt/Mo_2C catalyst can be activated by a mild reduction pretreatment dramatically improves the prospects of this catalyst for commercial application and a manuscript on this finding is in preparation.

Au/MgO

MgO is an attractive support because its simple NaCl crystal structure simplifies DFT calculations and provides a path for combination of experimental and computational results that can facilitate understanding of the structure and catalytic relevance of the metal/oxide three phase interface for water-gas shift. Due to the high point of zero charge for MgO, it is difficult to synthesize Au/MgO using our conventional deposition-precipitation NaOH method. We have successfully synthesized Au/MgO and Au/$Mg(OH)_2$, however, using a deposition-precipitation method with urea. As illustrated in Table 2, both Au/MgO and Au/$Mg(OH)_2$ showed similar kinetics except for the apparent order with respect to H_2O. Au/MgO showed a lower apparent H_2O order of 0.7±0.1 while Au/$Mg(OH)_2$ showed H_2O order 1.0±0.1. This implies a higher H_2O/OH coverage over the Au/MgO compared with Au/$Mg(OH)_2$, and corresponds to the higher rate found on Au/MgO. We note that both catalysts showed similar WGS rates per mole of Au (~$1x10^{-3}$(mol H_2)(mol Au)$^{-1}s^{-1}$ at 180 ^oC), but TEM showed a larger number-average Au particle size of Au/MgO (4.0±0.9 nm) versus Au/$Mg(OH)_2$ (2.2±0.7 nm). Since WGS rate decreases significantly as Au particle size increases, Au/MgO is deduced to have a higher rate for WGS at the same Au particle size. A kinetic isotope effect (KIE) of 2.0±0.3 for both catalysts implies the same reaction mechanism on both.

Table 2. Comparison of WGS Kinetic Data for Au supported on different metal oxides

Support	Au loading (wt%)	Test Temperature (°C)	WGS Rate per mole of Au at 180°C (mol H_2/mol Au/s)	E_a kJ/mol	H_2O	CO_2	CO	H_2	Average particle diameter (nm)
$Mg(OH)_2$	2.4	220	$8.0x10^{-4}$	29	1.00	-0.27	0.80	-0.31	2.2±0.7
MgO	2.4	220	$9.0x10^{-4}$	28	0.74	-0.26	0.86	-0.35	4.0±0.9
Al_2O_3	1.3	180	$2.9x10^{-3}$	12	0.81	-0.09	0.87	-0.36	2.1±0.5

To investigate the surface OH groups, operando FTIR was performed on Au/MgO under the same condition as that of WGS kinetics measurement (6.8% CO, 21.9% H_2O, 8.5% CO_2, 37.4% H_2, and balance Argon). The spectra are shown in Figure 2a. The peak at around 3700 cm^{-1} is assigned to hydroxyl groups. The peaks at around 1040 cm^{-1} and 1500 cm^{-1} are assigned to carbonate species, while those at 2730 and 2830 cm^{-1} are assigned to formate species. During stabilization, the peak area of the hydroxyl groups decreased with time while the WGS rate per mole of Au also decreased. The correlation between WGS rate and different IR peaks are shown in Figure 2b. The WGS rate showed a positive correlation with hydroxyl group IR peak area, which implies the participation of the hydroxyl group in the rate-determining step and predicts that a higher hydroxyl coverage will result in a higher WGS rate. This is consistent with DFT calculation results. Recent studies have shown that the 3700 band is significantly stronger when Au is present on the MgO surface and that its reactivity with CO requires the presence of Au. Thus, these species appear to be concentrated at the Au/MgO interface. A manuscript on this work is in the final stages of preparation.

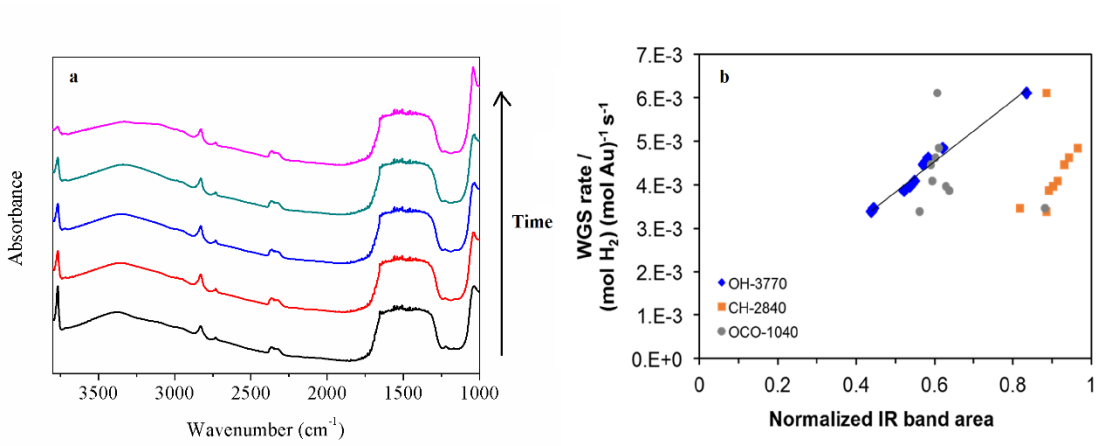

Figure 2. Operando FTIR of Au/MgO under WGS conditions. a) IR spectra, b) WGS rate correlation with IR peak areas.

Computational Modeling of Metal-Oxide interfaces

The emergence of density functional theory (DFT) based models over the past few decades has enabled great progress in rational catalyst design, especially for extended surfaces of transition metals [J. K. Nørskov, Abild-Pedersen, F., Studt, F., & Bligaard, T. (2011). *PNAS*, 108(3), 937–943]. However, insights from common metal-only slab models do not always translate well to metal nanoparticles dispersed on high surface area supporting phases. The water-gas shift reaction is a prominent example of a reaction in which the nature of the metal and support both have a substantial influence on catalytic

activity [Shankar et al. 2012, Williams, W. D.; Shekhar, M.; Lee, W.-S.; Kispersky, V.; Delgass, W. N.; Ribeiro, F. H.; Kim, S. M.; Stach, E. A.; Miller, J. T.; Allard, L. F., *J. Am. Chem. Soc*. 2010, *132*, 14018], and a metal-only model fails to capture observed rates [Clay et al. *J Catal* 2014].

In recognition of the limitations of the metal-only models, our recent project efforts focused on developing and characterizing supercell models of the metal-support interface. While there have been numerous DFT investigations of particular metal/oxide combinations in the context of a particular reaction (CO oxidation on Au/titania is a prominent example[Green, I. X.; Tang, W.; Neurock, M.; Yates, J. T., *Science* 2011, *333*, 736–739; Saavedra, J.; Doan, H. A.; Pursell, C. J.; Grabow, L. C.; Chandler, B. D., *Science* 2014, *345*, 1599–1602]), to-date there have been no efforts to develop more general models or to explore the types of scaling relations that have proved so powerful for understanding metal-only behavior [Abild-Pedersen, F.; Greeley, J.; Studt, F.; Rossmeisl, J.; Munter, T.; Moses, P.; Skúlason, E.; Bligaard, T.; Nørskov, J., *Phys. Rev. Lett.* 2007, *99*, 016105]. To this end, we turned to the quasi-one-dimensional nanowire configuration (Fig. 3), originally proposed by Molina and Hammer [Molina, L. and Hammer, B. (2003). *Phys. Rev. Lett.*, *90*, 206102], which offers a simple and uniform structural template that avoids the complicating finite size effects of (sub)nanometer particle models. We chose MgO(100) as a structurally and electronically simple, non-reducible metal oxide and have studied Au/MgO, the modification of the support, and the effects of nanowires of the late FCC transition metals (Rh, Ir, Pd, Pt, Ag, Au) most common to heterogeneous catalysis.

For studies of Au/MgO, to complement the experimental kinetic measurements, we have used a combination of periodic Density Functional Theory (DFT) calculations and detailed microkinetic modeling to elucidate the impact of the Au/MgO interface on the molecular-level features of water-gas shift chemistry. The nanowire structure allows us to avoid unnatural quantum size effects associated with small gold clusters while preserving a tractable simulation size. The results conclusively demonstrate that the barrier to activate water, which is prohibitively high (~2 eV) on a clean Au(111) surface, is decreased to essentially zero at the Au/MgO interface. The well-known carboxyl mechanism is found to be the most energetically favorable pathway at the interface, and with the dramatic reduction of the water activation barrier, this step is no longer rate limiting. Based on these DFT-calculated energetics and appropriate entropy estimates, a dual-site microkinetic model of the Au/MgO interface has been constructed. Rate control analysis clearly demonstrates both the high degree of kinetic control of COOH formation at the interface, and that the competitive adsorption between CO and H at the interface strongly influences the reaction kinetics. By introducing a systematic approach to refine the microkinetic predictions, in which the calculated energetics of kinetically sensitive steps are iteratively replaced with high accuracy predictions from hybrid HSE06 calculations, rapid convergence of key kinetic parameters is achieved. The determined effective activation barriers and reaction orders agree very well with both the results of predictions made with full HSE06 calculations and with our measured reaction orders and apparent activation barriers. This work is nearly ready for submission for publication.

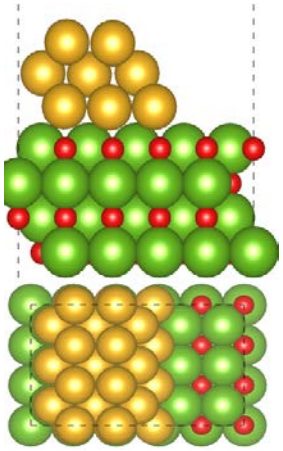

Figure 3. Top and side views of quasi-one dimensional Au/MgO nanowire model for WGS calculations.

The determination of a full kinetic model for WGS at the Au/MgO interface is an important first step in the establishment of reactivity trends at more general metal/oxide interfaces. However, rigorously

establishing and quantifying such trends requires systematically permuting the metal and the oxide. The former strategy is described in more detail below, while the latter approach can be explored by introducing near-surface substitutional cationic dopants into the MgO lattice. Such dopants can, in turn, alter the electronic structure of the oxide and thereby change important catalytic properties such as adsorbate binding energies and elementary reaction barriers.

We have explored the effect of a series of low and high valence dopants, including Li, Na, Al, Si, P, Ti, Mn, Fe, Co, Ni, Zn, Zr, Nb, Hf, Ta, and W, on the thermodynamics of the water-gas shift reaction at the Au/MgO interface. The dopant positions are optimized in the near-surface region, with most dopants preferring to substitute for Mg cations directly beneath the Au nanowires. The binding energies of the key intermediates for the WGS reaction, O, OH, H_2O, COOH, HCOO, and CO, are subsequently calculated for each of the doped systems. To provide more general information about trends in adsorbate binding energies at the metal/oxide interfaces, the binding energies of additional adsorbates that are not directly related to WGS, including OOH, CHO, CH_2O, CH_3OH, N, NH, NH_2, S, and SH, are also evaluated. Remarkably, the binding energies of these intermediates follow a series of scaling relationships that closely resemble similar relationships that have previously been established on simple metal surfaces. For example, as shown in Figure 4, the binding energies of OH and O (both adsorbed at the Au/MgO interface) follow a linear relationship with a slope of 0.66. Similar relationships have been found to exist between OOH and O binding energies, as well as H_2O and O, SH and S, NH and N, NH_2 and N, and O_2 and O. These results mark the first time, to our knowledge, that adsorbate scaling relationships have been identified at metal/oxide interfaces. Such relationships have proved to be a powerful tool in the development of volcano plots and computational catalyst screening strategies on single crystal metal surfaces, and it is possible that they will similarly facilitate the development of rapid catalyst screening techniques for oxide-supported metal nanoparticles. This work enables exploration of how the scaling relationships can be used to develop rigorous volcano plots for WGS at doped Au/MgO interfaces, and opens the way for determination of the extent to which these new relationships may be developed for other metal/oxide combinations.

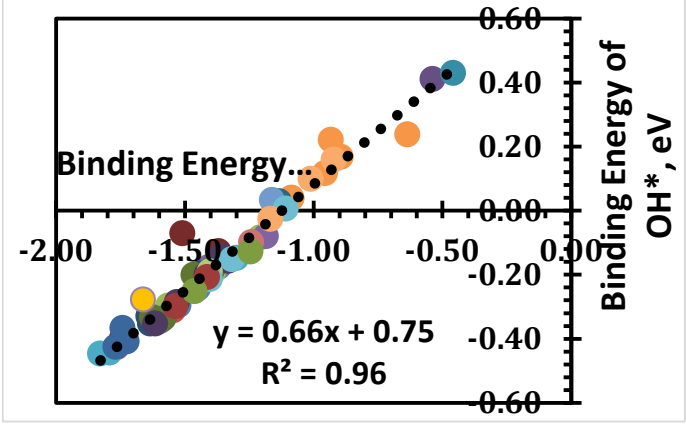

Figure 4. Scaling relationship of OH and O binding energies at doped Au/MgO interfaces. The different colors represent different dopants substituted in the near-surface region of the Au/MgO slabs.

We computed the adsorption of homologous series of species (CH_x, NH_x, OH_x) across all metals and at the perimeter sites of the metal-metal oxide interface. As an illustrative example, the adsorption configuration of NH_2 at the metal oxide interface is shown in Fig. 5 (inset). Most adsorbates prefer to bind in a configuration that involves coordination with two metal atoms and an Mg atom at the interface. Fig. 5 plots computed adsorption energies at the perimeter sites against the metal-only boundary sites. Significant positive and negative deviations are evident, which through a series of intermediate tests we we have traced to a combination of steric, strain, and d-band shifts largely determined by the nanorod

model, convoluted with a redox energy specific to the metal-metal oxide junction. We next tested the implications of these effects on the familiar linear scaling of homologous binding energies with the binding energy of the parent heavy atom (C, N, O) to a metal surface. The blue points in Figure 6 show that adsorbates bound at the perimeter of an unsupported nanowire, free of the effects of a support, exhibit nearly linear scaling across metals. The green points in Figure 6 show that this linear scaling is disrupted by the support: some points are shifted dramatically due to strong redox effects, while others are perturbed such that both the slope and intercept of a linear fit are shifted relative to the support-free system. These results highlight and quantify the underlying physics associated with reactivity changes at a metal-metal oxide interface and the potential to tune reactivity at these interfaces.

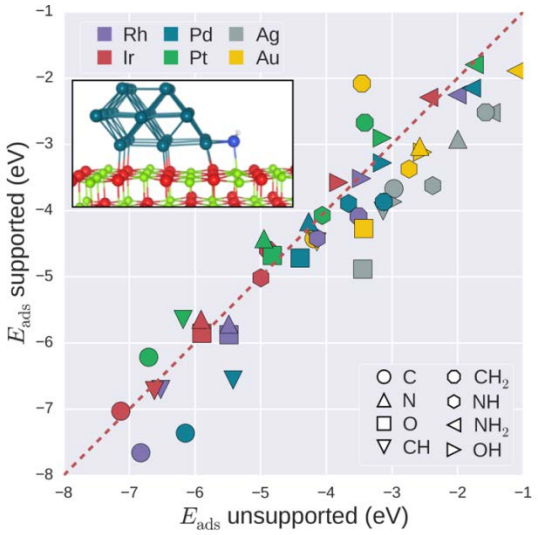

Figure 5. Parity plot between adsorption energies at the boundary of supported and unsupported nanowires. Inset: End-on view of (semi-infinite) Pd nanowire on MgO(100). Also shown is an NH2 intermediate adsorbed at the metal-oxide boundary.

The nanowire model is somewhat cumbersome for application across a large number of metal/oxide combinations. A simpler description of the modification of the oxide by the metal is provided by "inverse" models, i.e., thin oxide films placed epitaxially on a metal support. These are inexpensive to incorporate within the periodic boundary conditions typically employed within DFT and facilitate experimental characterization using surface science techniques. Figs. 7(a-b) show the electron density difference plots for F adsorption on oxide sites on the Ag/MgO nanowires and MgO thin films on Ag. It is evident that the perturbation in the electron density is very similar for both models. We note that these electronic perturbations originate from a redox coupling between the metal and the adsorbate, and are not observed for adsorption on the bulk oxide surface. Odd electron adsorbates are most affected by the metal-oxide interface, while the adsorption of molecules or species with low electron affinity (or ionization potential for electron donors) remain unaltered compared to the bulk oxide surface. In addition, we have found that adsorption energies of all electron acceptors/donors on oxide sites of the metal-oxide interface scale with the charge state of the adsorbate. Our findings indicate that a two pronged approach, with initial screening done on simple metal-only and supported oxide ultra-thin films, followed by detailed microkinetic studies with the nanowire model, could be an efficient strategy for applying a discovery informatics approach to supported particles.

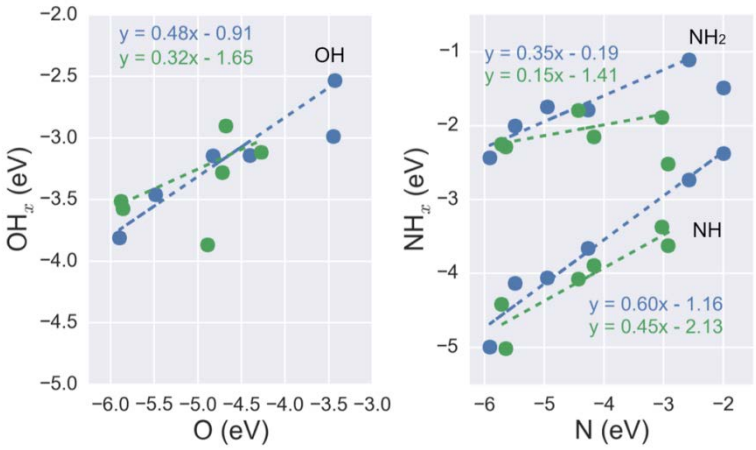

Figure 6. Comparison of scaling relations for adsorption at the perimeter of unsupported (blue) and MgO supported (green) nanowires.

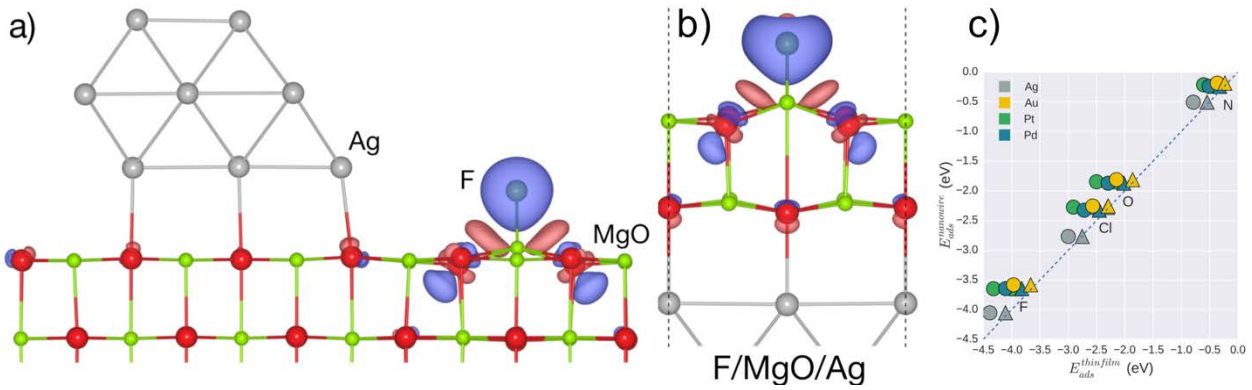

Figure 7. Comparison of adsorption on MgO sites on (a) nanowire model and (b) oxide thin-film model. Blue and red isosurfaces indicate charge accumulation and depletion respectively. (c) Parity plot of adsorption energies of different intermediates on the two models. Circles and triangles indicate film thicknesses of 2 and 3 ML respectively.

We also applied the nanowire model to WGS intermediates at a Pd/Al_2O_3 interface, focusing in particular on the sensitivity of model predictions to key nanowire/oxide choices, including metal/oxide registry, nanorod thickness, and metal and oxide terminations. Results are unexpectedly sensitive to the termination of the *bottom* of the oxide slab. Bulk termination, as is commonly applied, creates dangling bonds at the bottom of the slab, associated artificial midgap states, and exaggerated binding of redox-active intermediates (H, OH, …). Saturation of these states (e.g., by relaxing the bottom of the slab) is essential for well converged results. With this knowledge in hand, we contrasted binding preferences of common WGS intermediates — CO prefers Pd, H_2O prefers oxide, and carboxyl (COOH) prefers boundary sites, for instance — and drew implications for WGS steps. Fig. 8 shows that the H_2O dissociation is much more facile on oxide than metal, that the interface is intermediate between the individual components, and that the redox effects described above facilitate separation and subsequent reactions of H and OH. These results are consistent with a significant contribution of support to WGS reactivity even on a non-reducible oxide and highlight the non-linear couplings that make it necessary to model the two in combination. We believe these systematic comparisons are essential to advancing DFT as a design tool for supported metal systems.

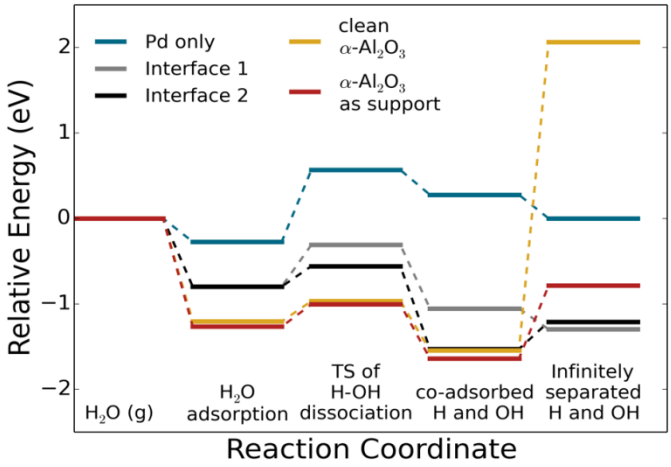

Figure 8. Potential energy surfaces of different water dissociation pathways at the Pd/Al2O3 interface.

Water activation on supported Pt catalysts using *Operando* IR and Isotopic Transient Techniques

The WGS TOR per surface metal on supported Pt catalysts (Pt/Al_2O_3, Pt/ZrO_2, Pt/CeO_2, $Na\text{-}Pt/Al_2O_3$, and $Na\text{-}Pt/TiO_2$) can vary by 100-fold depending upon the metal oxide support, which plays a direct role in activating water. Time-resolved IR spectra collected during transient H_2O/D_2O isotope switching revealed that the evolution of isotopically-labeled surface hydroxyl groups and molecularly-adsorbed H_2O

correlate with the WGS TOR, while formate (HCOO*) intermediates are spectator species for all supported Pt catalysts tested under these WGS conditions. These experiments have shown that the coverage of deuterium-containing active intermediates, which correspond to sites participating in water activation, can range from 0.03 (mole D) (mole surface Pt)$^{-1}$ on Pt/Al_2O_3 up to 2.4 (mol D) (mole surface Pt)$^{-1}$ on Pt/Al_2O_3 at 250 °C and 7% CO, 11% H_2O, 9% CO_2, 37% H_2. On Na-free samples, there is a normal H/D kinetic isotope effect (KIE), which ranges from 2.2 on Pt/Al_2O_3 to 2.6 on Pt/CeO_2. The inverse relationship between the apparent H_2O order and WGS TOR on these samples along with the measured H/D KIE suggests that supports with a higher surface coverage of OH exhibit higher rates since O-H bond breaking is rate-limiting on Na-free Pt. For Na-promoted Pt samples (Na-Pt/Al_2O_3, Na-Pt/TiO_2), the lower H/D KIE of 1.2 – 1.4 and higher apparent H_2O order (~1) suggest that the WGS TOR is no longer sensitive to the support in the presence of alkali, but is instead dependent on the Na loading. These results combined with previous experiments to measure the coverage of carbon-containing intermediates [Cybulskis, *J Catal*, 2016] show that Na promotes the WGS TOR on supported Pt catalysts by providing greater accessibility of surface OH/H such that all of the CO adsorbed on the exposed Pt surface is able to participate in the reaction. A paper on this work is in preparation.

Single-Pt-Atom-Free Pt/TiO_2 and Na Promoted Pt/TiO_2

While the promotion of Pt by Na is now well known, the role of Na is not clear. There are reports in literature claiming that the promotion is due to the formation of single Pt atoms in presence of Na. Here Pt nanoparticles were prepared and loaded onto TiO_2. STEM results confirmed the absence of single Pt atoms. Na was loaded onto the Pt/TiO_2 by incipient-wetness impregnation. The WGS kinetics results in Table 3 show that Na could still promote the activity of the Pt/TiO_2 sample and also changed the kinetics even though no single Pt atoms were present. These results imply that the single Pt atom formation is not the reason for the Na promotion effect. Instead, addition of Na creates a new type of site at the Na-Pt interface. As discussed above in the presentation of the isotopic transient results, we conclude that these new sites promote water activation.

Table 3. WGS kinetics of single Pt free Pt/TiO2 sample with and without Na

Catalyst	Temp ./ °C	Eapp/k J(mol)$^{-1}$	WGS rate per mole of Pt at 300 °C (10^{-2}/s)	H_2O	CO_2	CO	H_2
2.49wt% Pt/TiO_2	210	70	11	0.52	0.06	0.26	-0.68
2.49wt% Pt-Na(1:10)/TiO_2	210	90	26.3	0.73	-0.11	-0.04	-0.16

Fe promotion of Au/Rutile (TiO_2)

The negative apparent order with respect to CO for Au/Fe_2O_3 (-0.7~-0.43) found in previous results implies much stronger CO adsorption on that catalyst compared to Au supported on other oxides. To pursue the possibility that Fe electronically modifies the CO adsorption strength on Au and thus changes the catalyst activity, we prepared a series of different Fe-doped rutile (TiO_2) supports loaded with ~1wt% Au by the deposition-precipitation method. WGS rate per mole of Au at 120 ^oC was promoted by a factor

of 4 for 1 wt% Fe content. Significant changes in kinetic parameters were observed at varying Fe contents. Apparent orders with respect to CO decreased (from 0.7 to -0.3) and apparent activation energy increased (from 53 to 98 kJ $(mol)^{-1}$) with Fe content increasing from 0 wt% to 5 wt%, leading to a maximum WGS rate versus CO order, Figure 9.

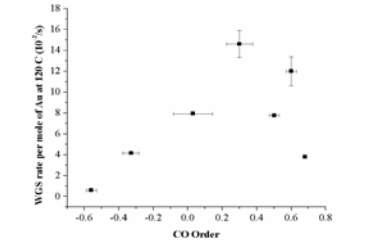

Figure 9. WGS rate versus CO order

Particle size distributions were obtained from Transmission Electron Microscopy (TEM) and the similar average particle sizes (2.0±0.5 nm) over all the catalysts excluded the particle size effects as the source of the maximum. Since decreasing CO order implies higher CO coverage and therefore stronger CO adsorption energy, the "volcano" in Figure 9 suggests an optimum CO binding energy. To examine the CO binding more closely, *operando* Fourier Transform Infrared Spectroscopy (FTIR) was performed on the 1 wt% Fe-doped catalyst and the result compared with Au supported on un-doped rutile. IR peaks at wavenumbers of 2097 cm^{-1}, 2015 cm^{-1}, 2044 cm^{-1}, 1967 cm^{-1} and 1888 cm^{-1} were observed. The peak at 2097 cm^{-1} can be assigned to CO adsorbed on metallic Au while the lower frequencies of 2044 cm^{-1} and 1967 cm^{-1} have been associated with CO adsorbed on sites with a higher degree of back donation and multiple bonding to the Au. The IR bands at frequencies below 2050 cm^{-1} were stronger than the corresponding peaks of Au supported on un-doped rutile (Figure 10) and thus suggest a participation of Fe in the neighborhood of the CO bonding site. The results show that Fe-doping can modify the CO adsorption properties of Au/Rutile and that WGS rates can be optimally promoted with appropriate Fe content. The nature of this promotion was investigated further with detailed FTIR and XAS studies and a manuscript is in preparation.

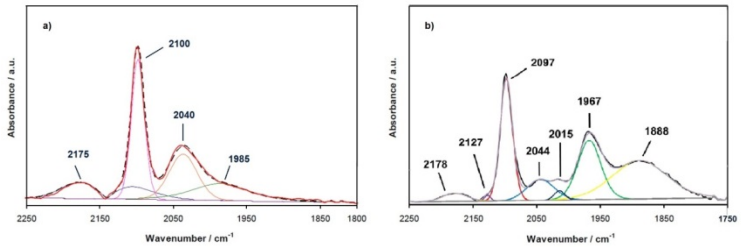

Figure 10. Comparison of the FTIR spectrum of a) Au/undoped-rutile; b) Au/1wt%Fe-rutile

Single-Site Olefin Polymerization

Although the bulk of α-olefin homogeneous catalysts have been modifications of well-understood metallocene motifs, designing and producing the next generation of nonmetallocene catalysts has proven to be a difficult task due to the variety of different possible structures. While the basic understanding of these catalysts has been significantly advanced in past years, there remains a lack of the mathematical relationships between catalyst structures and reactivity that is needed for predicting chemical reactivity and optimizing catalyst configurations.

Utilizing a family of Group IV amine bis(phenolate) complexes first reported by Kol and coworkers in 2000 (Figure 11), we have exploited the diverse reactivity and simple synthesis of these catalysts to create a range of different complexes. By focusing on this specific family of catalysts, we have shown the key effects of ligand and metal center variations on different olefin substrates. These key findings should offer applicable, useful comparisons to other structurally similar catalyst structures and offer new synthetic targets for product-specific catalysts.

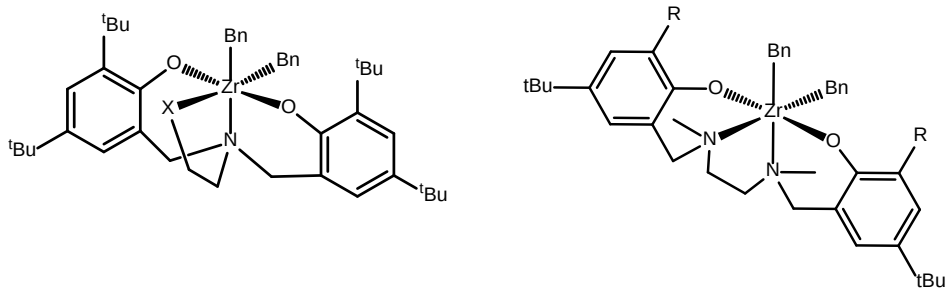

Figure 11. Structure of two amine bis(phenolate) architectures studied by our group.

The overall goal of this project has been focused on discovering quantifiable relationships between catalyst structures in order to predict new catalyst reactivity. This difficult task is compounded by the large number of possible reactions that can occur, the lack of modeling tools used currently in the scientific community in this area, and the difficulty of finding these mathematical relationships, also known as chemical descriptors, between kinetic data and catalyst. Outlined below is a summary of the work we have done in advancing the understanding of these relationships under this grant.

Kinetic Modeling of 1-Hexene Polymerization Catalyzed by Zr(^{t}Bu-ON^{NMe2}O)Bn$_2$/B(C$_6$F$_5$)$_3$

In order to determine chemical descriptors between catalyst structure and catalyst reactivity, we have created an analytical toolset that combines time-dependent data sets of monomer consumption, polymer termination by vinyl formation, steady-state analysis of active catalyst sites, and molecular weight distributions (MWD) of polymer. By analyzing all of these data sets simultaneously through a code of ordinary differential equations, we are able to optimize the individual rate constants to an accuracy that matches the polymer MWD over the course of the reaction (Figure 12). This process has been presented in Macromolecules (2012) and shows how analysis of each of these data sets is required to fully understand the polymerization mechanism. A key and unexpected finding in this report is that the participation of active catalyst species is much less than the initial catalyst loading. Without properly using this kind of analysis, it is impossible to accurately compare different catalysts. With this analytical toolset for kinetic analysis, however, we have been able to extract quantitative rate constants for key reaction rates, such as, chain transfer, propagation, misinsertions, tacticity, oligomerization, and even revealed new, unpredicted chemical reactivity in this field.

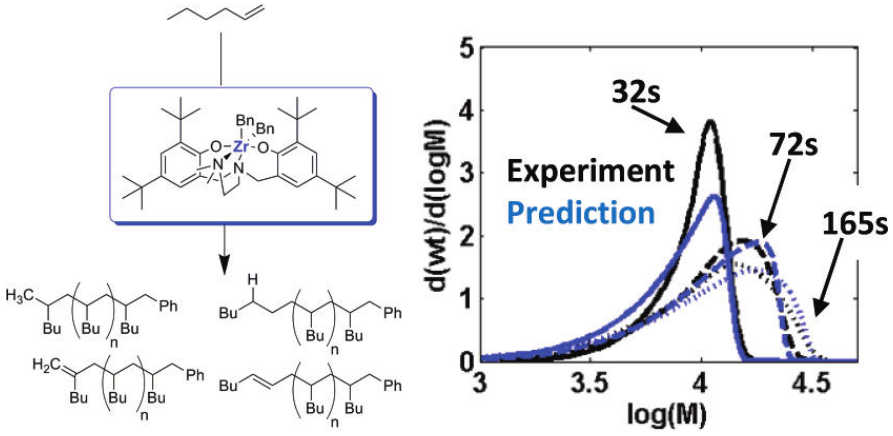

Figure 12. Experimental MWDs vs. predicted by our kinetic modeling method.

Zwitterionic Ring-Opening Polymerization: Models for Kinetics of Cyclic Poly(caprolactone) Synthesis

This analytical toolkit has also been applied successfully in other polymerization processes, such as in the ring-opening polymerization of caprolactone by NHC's, as in the 2014 Macromolecules paper from our group. In this study, we revealed several key insights on the rate of zwitterionic ring-opening polymerization of caprolactone and the reaction steps responsible for the time evolution of molecular weights and polydispersities. Simultaneous modeling of both the evolution of monomer conversion, molecular weights and molecular weight distributions were necessary to rule out several likely scenarios, as several models were adequate to model the rate of monomer conversion alone. On the basis of modeling, a minimal set of reaction steps was identified that could rationalize both the rates and molecular weights of the resulting cyclic poly(caprolactones), as well as the variations in rate caused by trace impurities. These studies revealed that the generation of reactive zwitterions by a slow and reversible initiation step is followed by the rapid growth of zwitterions. Initiation and propagation is accompanied by several chain-transfer and chain-scrambling steps, including the intramolecular backbiting of the alkoxide chain-ends on internal esters of the growing zwitterions to liberate cyclic chains, and the attack of active zwitterions on the internal esters of other zwitterions as well as cyclized chains (Figure 13). The attack of active zwitterions on cyclized chains is proposed as a key step that leads to high molecular weight cyclic poly(caprolactones).

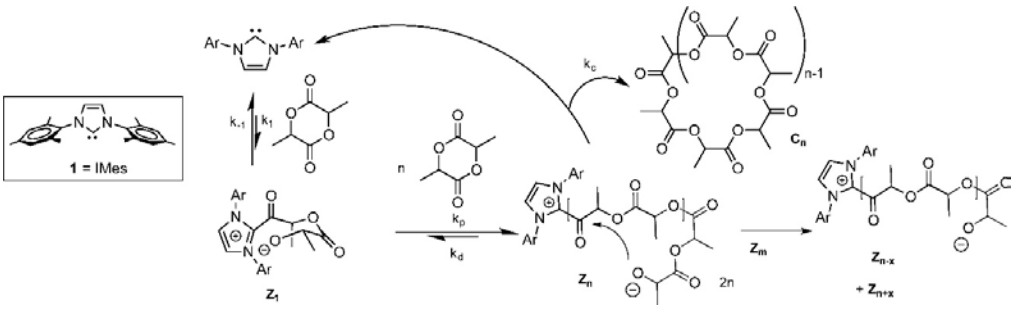

Figure 13. Mechanism of ring-opening polymerization of caprolactones by NHCs.

Effects of Pendant Ligand Binding Affinity on Chain Transfer for 1-Hexene Polymerization Catalyzed by Single-Site Zirconium Amine Bis-Phenolate Complexes

One of the salient factors in the conversion of olefins to larger products is the rate of chain termination, k_{ct}, that ends the growth of the polymer chain by separating the hydrocarbon product from the active metal center. By synthesizing a series of Zr catalysts with varying Lewis base pendants, we have determined a quantitative structure-activity relationship (QSAR) between the distance between the metal center and the pendant (M-X) for the monomer-independent, vinylidene formation rate constant, $k_{vinylidene}$. This was repeated with catalysts containing identical ligands with other Group IV metal centers (Figure 14). Furthermore, catalysts containing pendants beyond a certain length show a complete change in mechanism – catalysts with larger M-X distances exhibit monomer-dependent, vinylidene chain transfer.

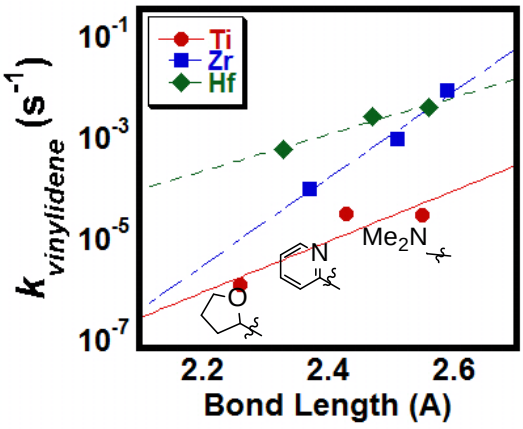

Figure 14. $k_{vinylidene}$ vs M-X bond length

In other work that is currently under review internally before journal submission, we see a similar relationship in synthetically similar Zr Salen catalysts. By varying the substituent size near the metal active site, a QSAR between the Sterimol minimum width (B_1) parameter and the monomer-independent, vinylidene chain transfer rate constant has been determined (Figure 15). The implication of this research is that the chain termination rate constants for these catalysts follow a predictable, quantitative pattern where decreasing steric bulk and increasing access to the metal center allows for increased rates of chain transfer. This finding allows for predictions to be made on the basis of catalyst sterics for synthesizing designer-catalysts that yield either increased oligomerization or living, long chain, polymerization. However, as we have shown, there are limits to this correlation and increasing the ligand size beyond a certain point may allow for a change in catalytic mechanism and require separate correlations to predict the magnitude of chain termination rate constants.

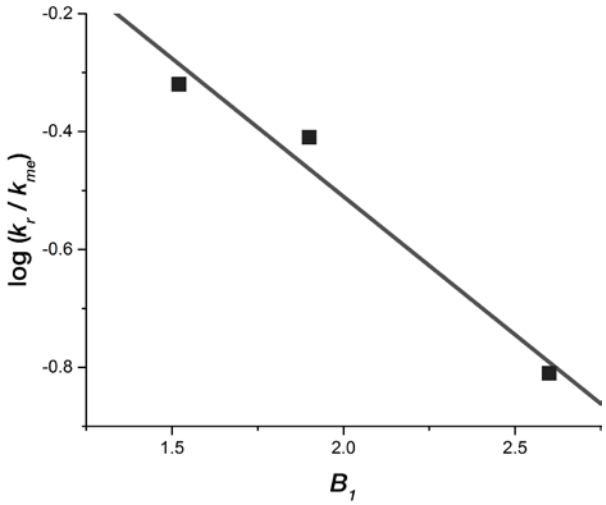

Figure 15. Comparison of *log* [$k_{vinylidene}$] versus the Sterimol minimum width (B_1) steric parameter

Effects of Metal and Lewis Pendant on Olefin Propagation

Another key parameter in the polymerization of olefins is the propagation rate constant, k_p. While other groups have reported that the sterics and electronics have had a pronounced effect on this rate constant, our work has shown two quantitative effects in both areas. In a comparison between the BF_3 Affinity of different Lewis bases and the k_p's for our different catalysts, which are depicted in Figure 16a, we see a remarkable trend in Figure 16b. This is not unexpected. One of our previous papers reports the effect of electronegativity of different substituents para- to a pyridine pendant catalyst on various rate constants [2013 ACS Cat paper], as shown in Figure 16c.

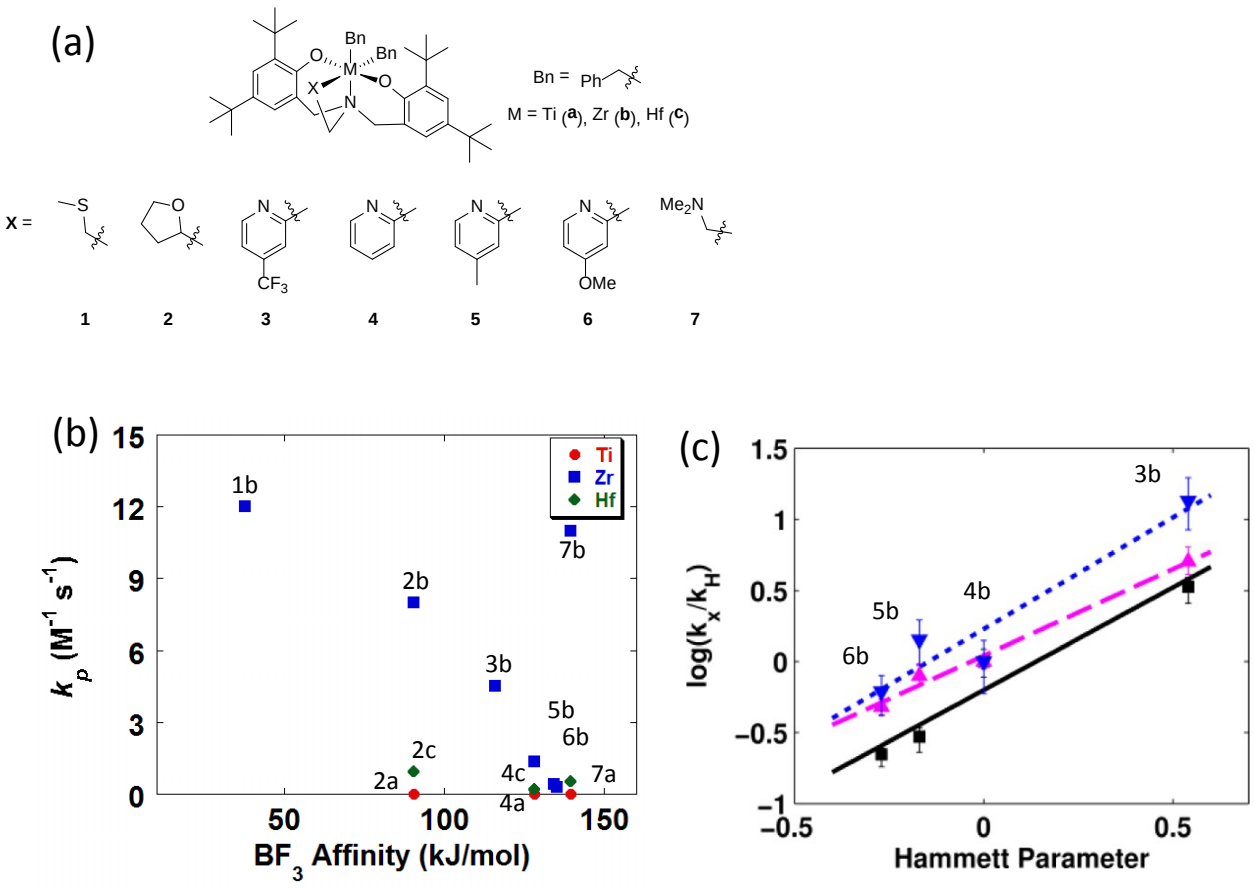

Figure 16. (a) Catalysts studied over the course of this grant (b) k_p vs BF_3 Affinity values of similar Lewis bases (c) Hammett plot of 3b-6b for k_p, black, k_{mis}, pink, and k_{rec}, blue.

In a subtle blend of electronic and steric factors, we observe that there is an order of magnitude difference between identical ligand systems containing different Group IV metals with the k_p trend of Zr > Hf > Ti. We can confidently state that the difference between Zr and Hf is due to electronic effects, since the catalysts are roughly the same size. Alternatively, the differences in k_p between Zr/Hf with Ti may have contributions to both electronics and sterics – the metal is much smaller, utilizing different frontier

orbitals, and pulls the ligand closer around the metal. Bringing the ligand structure closer reduces the effective active site area that is available to interact with incoming monomers. With regard to catalyst sterics, we have found that propagation rate constants for Salen catalysts show a linear dependence in a plot of the logarithm of the rate constants versus the Sterimol minimum width parameter, B_1, Figure 17. Such correlations should be able to help design and predict the overall activity for new catalyst synthesis.

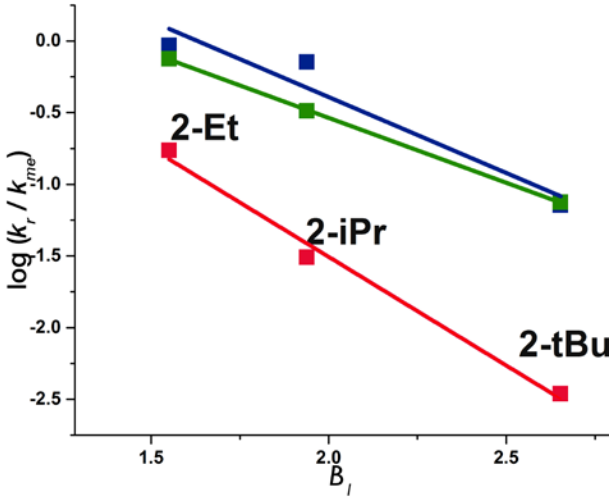

Figure 17. Insertion rate constants for propagation (blue), misinsertion (green) and initiation (red) compared to the Sterimol minimum width (B_1) steric parameter.

Effect of Metal and Ligand Structure on Misinsertions

In a reaction related to the propagation step for α-olefins, the misinsertion reaction is an important step that is involved with catalyst dormancy, formation of regioerrors, and the chain termination reaction producing polymers containing vinylene groups. In nearly all Group IV polymerization catalysts, the propagation step occurs through 1,2-insertion of the olefin. The alternative 2,1-insertion is considered an off-cycle step that reduces the overall catalyst activity. In fact, our work with Ti[THF] shows that this catalyst has equal amounts of active sites which have the last insertion as 1,2 and which have the last insertion as 2,1. With catalyst participation of ~20%, this means that the number of active catalysts is actually ~10%.

The formation of misinserted sites depends on the misinsertion rate constant, k_{mis}. The magnitude of this rate constant can be influenced by the electronegativity of constituents as seen by our 2013 ACS catalysis work, shown above in Figure 16c. We determined that the identity of the metal center changes the ratio of the $k_{misinsertion}/(k_p + k_{misinsertion})$. As we go down the periodic table, we see a qualitative decrease in this ratio as we go from Ti to Zr to Hf. We propose that the electron density at the active site has a direct effect on this ratio, where the electron poor Ti shows the most misinsertions and the relatively electron rich Hf produces the least amount of misinsertions relative to propagation.

Furthermore, using our knowledge that increased catalyst sterics decreases chain termination, we see that the formation of regioerrors, an error in the polymer chain where a dormant site returns to the catalyst cycle by a 1,2-insertion of monomer, follows the trend with increased regioerrors for the sterically bulky, Ti catalysts (~1-5%) and fewer regioerrors for the more sterically accessible Zr (.50%) and Hf catalysts (~.12%). The results of this are shown in conjunction with regioerrors reported for similar catalysts in Figure 18. The Zr and Hf catalysts choose to terminate the 2,1-inserted site and produce polymers with

reduced MWD. Controlling for these reactions by changing the metal center has proven to be important for the producing highly isotactic polypropylene on metallocene catalysts.

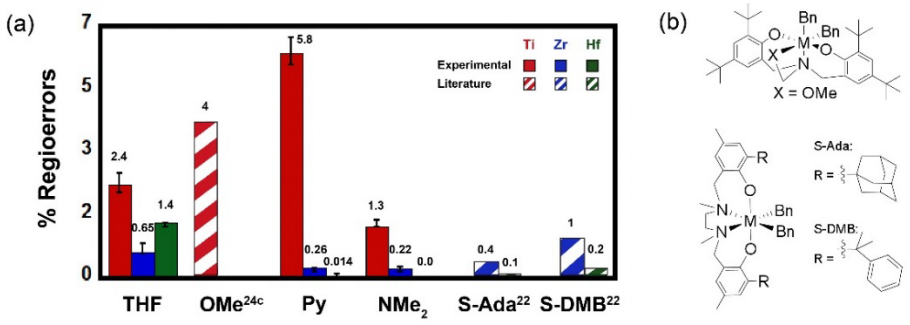

Figure 18. Percent of regioerrors for multiple group IV catalyst systems.

Effect of Ligand Design on Polymer Tacticity

Another important factor related to the propagation rate constant is the tacticity of the resulting polymer. In many cases, it is very desirable to design catalysts that can produce highly isotactically enriched polymers, as the degree of isotacticity has a great impact on the overall crystallinity of the polymer. One of the most commonly utilized methods to produce isotactically rich polymers is the synthesis of chiral catalysts with bulky groups near the active site to direct the 1,2-insertion of α-olefin. In our work with Zr Salen catalysts, we can quantitatively correlate the relative size of the substituents near the active site with the isotactic enrichment within the polymer, Figure 19.

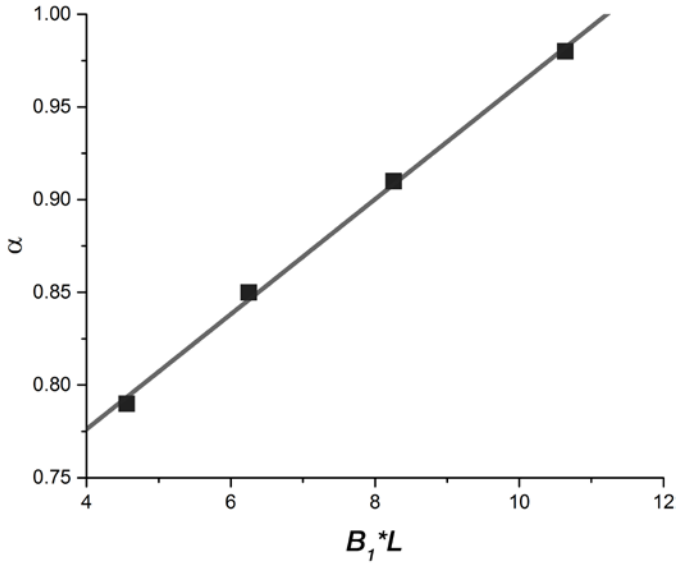

Figure 19. Comparison of the enantioselectivity of each catalyst (α) with the Sterimol steric parameters for minimum length (B_1) and length (L) of the substituent.

In Figure 19, B_1 and L are the Sterimol steric parameters for the minimum width and the length of the substituent, respectively. The enantioselectivity parameter, α, was calculated from the relative

concentration of the *mm* triad by ^{13}C NMR. By this analysis, we have proven that tacticity is induced in these catalysts through a site-control type mechanism, and can be controlled in a linear fashion through increasing the size of the substituent in both length and width.

Observance of Chain Walking in Zr[Pr]

Following the trend that we saw with increasing chain transfer with increasing M-X distance, we synthesized and began reactivity studies using a Zr catalyst that contained a propyl pendant (Zr[Pr]), i.e. a pendant without a coordinating Lewis base. Initial testing with the tris(pentafluoroaryl)borane, $B(C_6F_5)_3$, activator showed a rapidly deactivating oligomerization catalyst. By changing the activator cocatalyst to a trityl tetrakis(pentafluoroaryl)borate, $CPh_3B(C_6F_5)_4$, we showed a stabilization of the catalyst-activator pair that produced 1-hexene oligomer products. Further reactivity studies with 1-dodecene showed similar oligomer product distributions, albeit with a higher percentage of vinylene terminated products when compared to the 1-hexene oligomers. Unexpectedly, this catalyst showed a propensity for chain walking. Chain walking is the reinsertion of a vinylidene chain end back into a M-H bond of the catalytic site. A subsequent β-hydride elimination forms a tri-substituted olefin chain end, the rate constant labeled below as k_{trisub}. We envision that the decreased steric bulk near the catalyst active site allows for the facile chain transfer and vinylidene chain walking. The catalyst structure and chain walking reactions are shown in Figure 20.

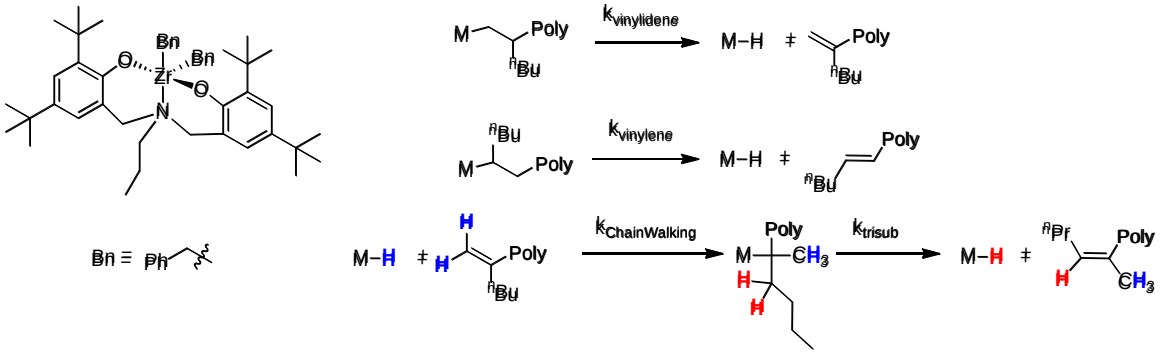

Figure 20. Zr[Pr] structure and chain termination/walking reactions

Kinetic Modeling of New and Emerging Mechanisms

Degenerative Benzyl Group Transfer

Using a previously studied zirconium amine bis-phenolate catalyst, Zr[tBu-ONTHFO]Bn2, the effect of substoichiometric amounts of activator on the polymerization was studied to more clearly elucidate the mechanism of degenerative benzyl-group transfer. Comprehensive kinetic analysis was performed over a range of activator to precatalyst ratios. The analysis determined the rates of association and dissociation of a binuclear complex (BNC) intermediate through which degenerative transfer proceeds (Figure 21). Kinetic modeling indicates that the benzyl-group transfer inside the BNC is rapid, as supported by ^1H NMR. Rapid association and dissociation of the BNC enable complete activation of all precatalysts even under the condition of substoichiometric amounts of activator through a degenerative benzyl-group transfer. Through the use of a novel experimental technique wherein a labeled catalyst is introduced during a normal polymerization reaction, this process was observed to instantaneously activate all

incoming precatalyst and effectively shut down the misinsertion pathway. The kinetic analysis showed that BNC has a faster initiation rate than a typical catalyst–ion pair, which may be due to the anion being previously displaced by the incoming unactivated precatalyst.

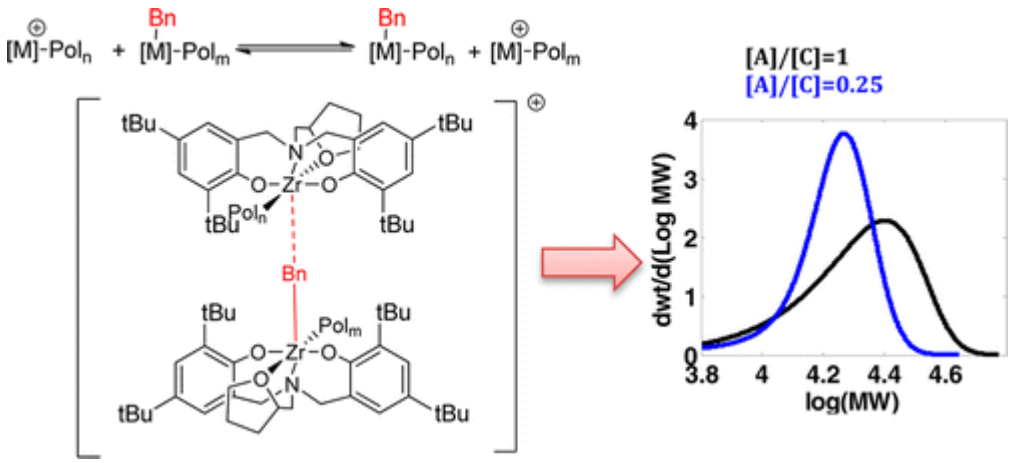

Figure 21. Mechanism for degenerative benzyl transfer, leading to far narrower PDI.

Observation of Dynamic Behavior in a Series of Group IV Amine Bis(Phenolate) Polymerization Catalysts

For this study, four Zr-based salan catalysts (Figure 22) were examined, and the rate constants for elementary steps in the catalytic mechanism showed a steric dependence. We have been able to experimentally prove the theorized dormancy states studied by Macchioni. Salan compounds have been hypothesized to possess dynamic behavior upon activation with a number of cocatalysts. For olefin polymerization, the catalyst can exist in two forms: the active form wherein the open coordination site is cis to the growing polymeryl (cis-active polymerization species or CAPS) and an inactive or dormant form wherein the coordination site and polymeryl are trans (trans-inactive polymerization species or TIPS). Furthermore, the effect is most prevalent in **1**, and is diminished as one increases the steric bulk of the ortho substituent, until it is completely absent in catalyst **4.** This was attributed to the destabilization of the TIPS form through steric crowding, as the ortho substituents begin to repel each other from the close proximity. This allows the CAPS form to be more favored as the size of the ortho position increases.

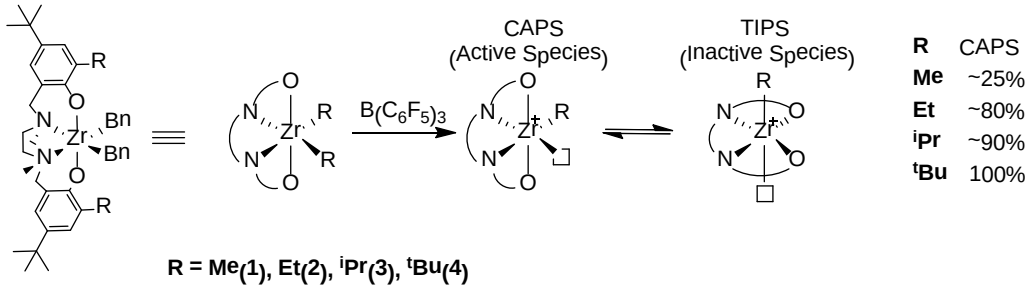

Figure 22. Reduced steric bulk leads to greater amount of dormant site formation.

Associative Tandem Oligomerization of 1-Hexene and Enchainment Polymerization by a Group IV Amine Bis(Phenolate) Catalyst

We employed our unique model based approach to study a group IV amine bis(phenolate) catalyst that is capable of simultaneously producing both oligomers of 1-hexene and polymers. Surprisingly, it was found that the polymer produced is structurally different from poly(1-hexene). Compelling evidence suggests that the polymer is partially composed of oligomers of 1-hexene. The polymer weight fraction was independent of conversion and was not affected by an increase in the concentration of free oligomers in the solution. We considered a number of mechanisms and the most plausible one that is supported by spectroscopic and kinetic data proposed that the dual polymerization and oligomerization behavior of the catalyst is due to the presence of two active sites which only differ in the pendant bond connectivity. We showed that the interaction between these two active sites facilitates the enchainment of oligomers on the oligomer site into the growing polymer chains of the polymer site. Using kinetic and thermodynamic control, we were able to tune the catalyst activation conditions to obtain exclusively oligomers or polymers, where the polymer structure could be varied from linear to branched poly(1-hexene). This phenomenon of two active sites originating from the same pre-catalyst and interacting with each other to make, in a controlled manner, oligomeric and polymeric products introduces a new branch of tandem catalysis that we have named Associative Tandem Catalysis (Figure 23).

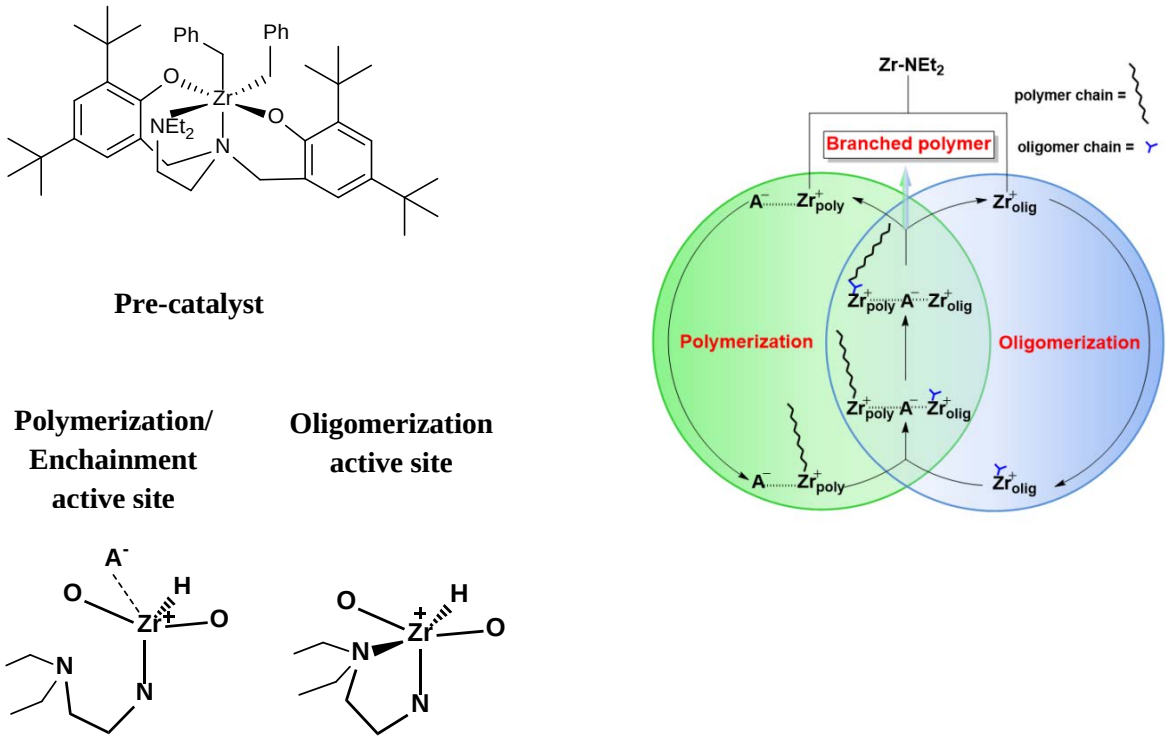

Figure 13. Summary of proposed catalytic mechanism, highlighting the oligomerization site with the pendant coordinated to the metal and the polymerization/enchainment site with the pendant detached.

In addition, we found that this catalyst produces oligomers with double-bond terminated (vinylidene) chains with at least 97% selectivity. To the best of our knowledge, this selectivity is higher than any other reported value for a post-metallocene olefin oligomerization catalyst. These α-olefin oligomers are, typically, highly branched and amorphous, possessing sufficiently high viscosity at higher temperatures

and good flow properties at low temperatures to make them ideal candidates to be used as synthetic lubricant base-stocks (eg: Mobil 1). In addition, 1-hexene oligomers can lead diesel and jet fuel. Finally, the end-groups can also be subsequently functionalized to yield chemicals that are intermediates in producing an array of products including adhesives, fragrances and surfactants.

Modeling and Activation Parameters for Zirconium Amine Bis(Phenolate) Catalysts

The chemical kinetics for a series of three zirconium amine bis(phenolate) catalysts for polymerization of 1-hexene was examined over a wide temperature range. Detailed modeling of the experimental data yielded the activation parameters for many of the reaction rate constants, including those for propagation, initiation, chain transfer, and monomer misinsertion and recovery (Figure 24). While existing literature is sparse, the results herein generally agree with previously published values, specifically that for the propagation rate constant the magnitude of the enthalpy of activation is low (below 13 kcal mol-1) and the magnitude of the entropy of activation is high (up to –22 cal mol-1 K-1). With regard to the remaining rate constants, for the reactions that have a more sterically crowded catalyst site due to the presence of a secondary carbon–Zr bond (recovery from misinsertion and vinylene formation) the magnitude of the activation entropy is high and the enthalpy is low, while for the reactions with a less sterically encumbered catalyst site due to the presence of a primary carbon–Zr bond (monomer misinsertion and vinylidene formation) the entropy is low and the enthalpy is high, excepting cases for vinylidene formation where steric crowding comes from other sources, such as the catalyst's pendant side chain. These results suggest that the rate determining step for each pair of reactions is different (docking of the monomer to the active site vs. bond formation). This difference in the rate determining step provides the ability to independently tune the parameters and create a more desirable polymer product.

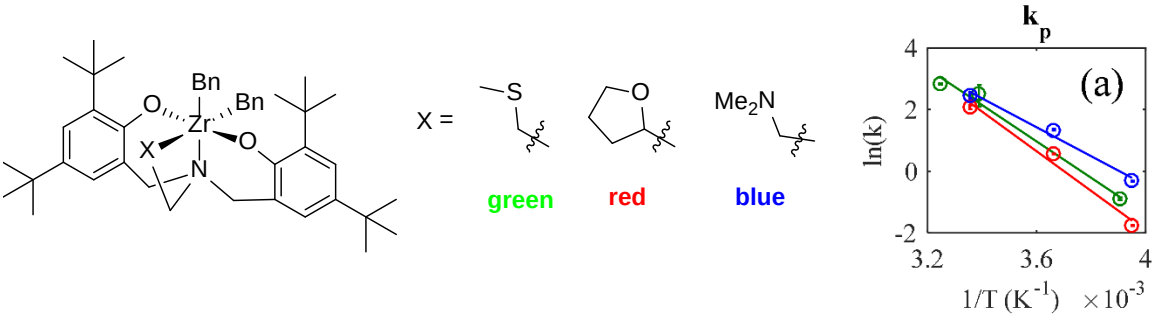

Figure 24. Temperature dependence on k_p illustrated by an Arrhenius plot.

Effects of Activator and Lewis Base on the Oligomerization and Polymerization of Olefins Catalyzed by a 5-Coordinate, Single-Site Zirconium Amine Bis-Phenolate

As we have shown in the previous discussion, there is a desire to design catalyst structures to produce polymers of vary lengths. Typically, this process has been done by synthesizing different catalyst structures that influence the ratio of k_p/k_{ct} (propagation rate versus the termination rate), where larger k_p/k_{ct} makes larger polymers and smaller k_p/k_{ct} produces oligomers. Recent work published by the Bercaw laboratory has shown a new method for controlling this ratio. They have shown that a 5 coordinate Zr catalyst featuring a carbene donor can switch from an oligomerization catalyst to a polymerization catalyst by coordinating a stoichiometric amount of trialkyl phosphine Lewis base to the catalyst. Expanding on this research, we have shown that the previously mentioned Zr[Pr]/$CPh_3B(C_6F_5)_4$ oligomer

catalyst system can be converted to a polymerization system by the addition of trialkyl phosphines. Furthermore, we have expanded this range of Lewis bases to include the first nitrile adduct. Using MeCN, polymers were produced with Mw similar to those by trimethyl phosphine (Figure 25). Such experiments may allow for on-demand control of polymeric products without requiring further synthesis by modulating the catalyst reactivity through the coordination of different Lewis bases.

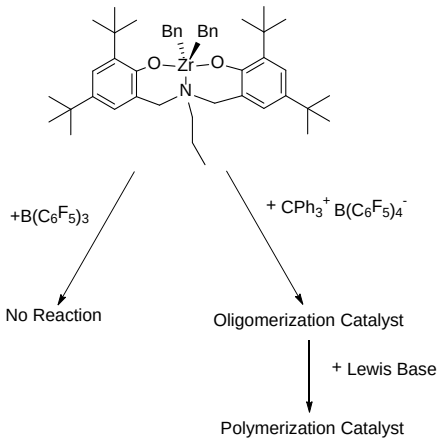

Figure 25. Activation of Zr[Pr] with $B(C_6F_5)_3$ results in no reactivity, while activation with $CPh_3B(C_6F_5)_4$ results in an oligomerization catalyst, followed by a polymerization catalyst upon addition of Lewis base.

Publications

1. Switzer, J.; Travia, N.; Steelman, D. K.; Medvedev, G.; Thomson, K.; Delgass, W. N.; Abu-Omar, M. M.; Caruthers, J. M. Kinetic Modeling of 1-Hexene Polymerization Catalyzed by Zr(tBu-ONNMe2O)Bn2/B(C6F5)3. *Macromolecules* **2012,** *45*, 4978–4988.
2. Shekhar, M.; Wang, J.; Lee, W.-S.; Williams, W. D.; Kim, S. M.; Stach, E. A.; Miller, J. T.; Delgass, W. N.; Ribeiro, F. H. Size and Support Effects for the Water-gas Shift Catalysis Over Gold Nanoparticles Supported on Model Al_2O_3 and TiO_2. *J. Am. Chem. Soc*. **2012**, 134, 4700–4708
3. Pazmiño, J. H.; Shekhar, M.; Williams, W. D.; Akatay, M. C.; Miller, J. T.; Delgass, W. N.; Ribeiro, F. H. Metallic Pt as active sites for the Water-Gas Shift reaction on alkali-promoted supported catalysts. *J. Catal.* **2012,** *286*, 279-286.
4. Wang, J.; Kispersky, V. F.; Delgass, W. N.; Ribeiro, F. H. Determination of the Au active site and surface active species via *operando* transmission FTIR and isotopic transient experiments on 2.3 wt% Au/TiO2 for the WGS reaction, *J. Catal.* **2012,** *289*, 171–178.
5. Williams, W. D.; Bollmann, L.; Miller, J. T.; Delgass, W. N.; Ribeiro, F. H. Effect of Molybdenum Addition on Supported Platinum Catalysts for the Water–Gas Shift Reaction. *Appl. Cat. B* **2012,** *125*, 206– 214.
6. Shekhar, M.; Wang, J.; Lee, W.-S.; Akatay, M. C.; Stach, E. A.; Delgass, W. N.; Ribeiro, F. H. Counting Au Catalytic Sites for the Water–Gas Shift Reaction. *J. Catal.* **2012**, *293*, 94–102.
7. Manz, T. A.; Caruthers, J. M.; Sharma, S.; Phomphrai, K.; Thomson, K. T.; Delgass, W. N.; Abu-Omar, M. M. Structure-Activity Correlation for Relative Chain Initiation to Propagation Rates in Single-Site Olefin Polymerization Catalysis. *Organometallics* **2012**, *31*, 602–618.
8. Steelman, D. K.; Xiong, S.; Pletcher, P. D.; Smith, E.; Switzer, J. M.; Medvedev, G. A.; Delgass, W. N.; Caruthers, J. M.;. Abu-Omar**,** M. M. Effects of pendant ligand binding affinity on chain transfer for 1-hexene polymerization catalyzed by single-site zirconium amine bis-phenolate complexes. *J. Am. Chem. Soc.* **2013**, *135*, 6280-6288.
9. Steelman, D. K.; Pletcher, P. D,; Switzer, J. M.; Xiong, S.; Medvedev, G. A.; Delgass, W. N.; Caruthers, J. M.; Abu-Omar, M. M. Comparison of Selected Zirconium and Hafnium Amine Bis(phenolate) Catalysts for 1-Hexene Polymerization. *Organometallics* **2013**, *32*, 4862−4867.

10. Clay, John P., Jeffery P. Greeley, Fabio H. Ribeiro, W. Nicholas Delgass, William F.Schneider, "DFT Comparison of Intrinsic WGS Kinetics over Pd and Pt", *J. Catal.*, **2014,** *320*, 106–117.
11. Xiong, S.; Steelman, D. K.; Medvedev, G. A.; Delgass, W. N.; Abu-Omar, M. M. ; Caruthers, J. M. Selective Degenerative Benzyl Group Transfer in Olefin Polymerization. *ACS Catal.* **2014**, *4*, 1162-1170.
12. Brown, H. A.; Silei Xiong, S.; Medvedev, G. A.; Chang, Y. A.; Abu Omar, M. M.; Caruthers, J. M.; Waymouth, R. M. Zwitterionic Ring-Opening Polymerization: Kinetic Models for the Synthesis of Cyclic Poly(caprolactones). *Macromolecules*, **2014**, *47*, 2055-2963.
13. Steelman, D. K.; Xiong, S.; Medvedev, G. A.; Delgass, W. N.; Caruthers, J. M.; Abu-Omar, M. M. Effects of Electronic Perturbations on 1-Hexene Polymerization Catalyzed by Zirconium Amine Bisphenolate Complexes. *ACS Catal.* **2014**, *4* (7), 2186-2190.
14. Sabnis, Kaiwalya D; M. Cem Akatay; Yanran Cui; Fred G Sollberger; Eric A Stach; Jeffrey T Miller; W. Nicholas Delgass; Fabio H Ribeiro, "Probing the Active Sites for Water-Gas Shift over Pt/Molybdenum Carbide using Multi-Walled Carbon Nanotubes," *J. Catal.*, **2015**, *324*,9-13.
15. Sabnis, Kaiwalya D., Yanran Cui, M. Cem Akatay, Mayank Shekhar, Wen-Sheng Lee, Jeffrey T. Miller, W. Nicholas Delgass and Fabio H. Ribeiro, "Water-Gas Shift Catalysis over Transition Metals Supported on Molybdenum Carbide." *J. Catal.*, **2015.** *331*, 162-171.
16. Cybulskis, Viktor J., Jun Wang, Jorge H. Pazmiño, Fabio H. Ribeiro, and W. Nicholas Delgass, "Isotopic Transient Studies of Sodium Promotion of Pt/Al_2O_3 for the Water-Gas Shift Reaction," *J. Catal*, **2016,** *339*, 163-172.

Papers Under Review

1. Pletcher, P. D.; Switzer, J. M.; Medvedev, G. A.; Delgass, W. N.; Caruthers, J. M.; Abu-Omar, M. M. Quantitative Comparative Kinetics of 1-Hexene Polymerization across Group IV Bis-Phenolate Catalysts. *ACS Catal.* Submitted.
2. Gunasekara, T.; Kim, J.; Xiong, S.; Preston, A. Z.; Steelman, D. K.; Medvedev, G. A.; Delgass, W. N.; Caruthers, J. M.; Abu-Omar, M. M. Associative tandem oligomerization of 1-hexene and enchainment polymerization by a group IV amine bis(phenolate) catalyst. *J. Am. Chem. Soc.* Submitted

Patent Applications

1. Gunasekara, T.; Kim, J.; Xiong, S.; Medvedev, G. A.; Delgass, W. N.; Caruthers, J. M.; Abu-Omar, M. M. Associative tandem oligomerization of 1-hexene and enchainment polymerization by a group IV amine bis(phenolate) catalyst. U.S. Provisional Patent Appl. 62/303,267, March 03, 2016.
2. Gunasekara, T.; Abu-Omar, M. M.; Caruthers, J. C. Olefin Oligomerization, Regio-selective Vinylidene Formation, Group IV Amine Bis(Phenolate) Catalyst, U.S. Provisional Patent Appl, 62/295,962, February 16, 2016

Manuscripts in Preparation

1. Preston, A. Z.; Kim, J.; Medvedev, G. A.; Delgass, N. A.; Caruthers, J. C.; Abu-Omar, M. M. Ligand substituent and solvation effects on activity, dormancy, and tacticity in a series of goup IV amine bis(phenolate) polymerization catalysts. *ACS Catal.*, Manuscript in preparation
2. Switzer, J. M.; Pletcher, P. D.; Steelman, D. K.; Medvedev, G. A.; Delgass, N. A.; Caruthers, J. C.; Abu-Omar, M. M. Modeling and activation parameters of selected zirconium amine bis(phenolate) catalysts for 1-hexene polymerization. *ACS Catal*., Manuscript in preparation
3. Pletcher, P. D.; Kim, J.; Medvedev, G. A.; Delgass, N. A.; Caruthers, J. C.; Abu-Omar, M. M. Effects of activator and Lewis base on the oligomerization and polymerization of olefins catalyzed by a 5-coordinate, single-site zirconium amine bis(phenolate) complex. *Organometallics*, Manuscript in preparation
4. P. Mehta, J. P. Greeley, W. N. Delgass, W. F. Schneider, "Correlations and Scaling Relations for Adsorption at the Metal-Oxide Boundary," J.Phys. Chem. Lett., Manuscript in preparation
5. P. Mehta, J. P. Greeley, W. N. Delgass, W. F. Schneider, "Comparison of Thin Film and Nanowire Models for Reactive Metal-Oxide Junctions," J. Phys. Chem., Manuscript in preparation
6. J. P. Clay, S. McDonough, K. Frey., J. P. Greeley, W. N. Delgass, W. F. Schneider, "Explicit and Mean-Field Models for Coverage-Dependent CO Adsorption on Pd," J. Phys. Chem., Manuscript in preparation
7. H. Zhu, P. Mehta, J P. Greeley, W. N. Delgass, Z. Zhao and W. F. Schneider, "Computational Characterization of a Pd/Al2O3 Nanowire Model for WGS," ACS Catal., Manuscript in preparation
8. Sabnis, Kaiwalya D., Yanran Cui, M. Cem Akatay, Jeffrey T. Miller, W. Nicholas Delgass and Fabio H. Ribeiro, "300ºC Activation of Pt/Mo_2C for Water-Gas Shift Catalysis." *J. Catal.*,In preparation.

9. Yanran Cui, Zhenglong Li, Zhijian Zhao, Viktor Cybulskis, Kaiwalya D. Sabnis, Chang Wan Han, Volkan Ortalan, Jeffrey Greeley, W. Nicholas Delgass and Fabio H. Ribeiro, Participation of Interfacial Hydroxyl Groups in the Water-Gas Shift Reaction over Au/MgO Catalysts, *J. Catal.* IN preparation.
10. Yanran Cui, Kaiwalya D. Sabnis, Cem Akatay, Viktor Cybulskis, W. Nicholas Delgass and Fabio H. Ribeiro; Fe Promoted Au/Rutile for the Water-Gas Shift Reaction, *J. Catal.* In preparation.
11. W. Damion Williams, Jeffrey P. Greeley, W. Nicholas Delgass, and Fabio H. Ribeiro, Water Activation and Carbon Monoxide Coverage Effects on Maximum Rates for Low Temperature Water-Gas Shift Catalysis, *J Catal.* In preparation.
12. Zhi-Jian Zhao, Houyu Zhu, Yanran Cui, William Schneider, W. Nicholas Delgass, Fabio H. Ribeiro, and Jeffrey P. Greeley, "Importance of metal-oxide interfaces in water-gas shift chemistry: a combined DFT, microkinetic, and experimental study of WGS on Au/MgO, J. Amer. Chem, Soc., in preparation